Trapping of Charge Carriers in Colloidal Particles of Self-Assembled Films from TiO_2 and Poly(vinyl sulfonic acid)

Nelson A. Galiote,[†] Antonio J. F. Carvalho,[‡] and Fritz Huguenin*[,†]

Departamento de Química, Faculdade de Filosofia, Ciências e Letras de Ribeirão Preto—Universidade de São Paulo, 14040-901 Ribeirão Preto (SP), Brazil, and Universidade Federal de São Carlos, Campus Sorocaba, C.P. 3031, 18043-970 Sorocaba (SP), Brazil

Received: July 21, 2006; In Final Form: August 31, 2006

Self-assembled electrodes consisting of TiO_2 nanoparticles and poly(vinyl sulfonic acid) (PVS) were prepared by the layer-by-layer (LbL) technique. The electrostatic interaction between the TiO_2 nanoparticles and PVS allowed the growth of visually uniform multilayers of the composite, with high control of the thickness and nanoarchitecture. The electrochemical and chromogenic properties of these TiO_2/PVS films were examined in an electrolytic solution of 0.5 M $LiClO_4$/propylene carbonate. The presence of two intercalation sites was noted during the positive potential scan, and they were attributed to different mobilities of charge carriers. Several charge/discharge cycles demonstrated the trapping of charge carriers in the TiO_2 sites. The absorbance change associated with the oxidation of the trapping sites was attributed to electronic transitions involving energy states in the gap band formed due to the strong distortion of the TiO_2 host. Using the quadratic logistic equation (QLE), it was possible to analyze the electronic intervalence transfer from Ti^{3+} to Ti^{4+}. Using the parameters obtained from this fitting, the amount of trapping sites in the LbL film was also determined. Electrochemical impedance spectroscopy (EIS) data gave the time constant associated with diffusion and the trapping sites. The diffusion coefficient of lithium ions changed from ca. 4.5×10^{-13} cm^2 s^{-1} to 3.0×10^{-14} cm^2 s^{-1} for all the potential range applied, indicating that PVS did not hinder the ionic transport within the LbL film. Finally, on the basis of the spectroelectrochemical data and scanning electron micrographs, the trapping effects were attributed to the colloidal particles of $Li_{0.55}TiO_2$.

Introduction

Among semiconductor materials, TiO_2 has been extensively applied in research because of its high chemical stability, nontoxicity, and low cost. TiO_2 electrodes have been applied to photoelectrochemical solar cells, photocatalytic devices, electrochromic and photoelectrochromic windows, and rocking-chair lithium battery.[1−6]

Recently, much attention has been focused on the use of nanostructured TiO_2 for these applications. These nanostructured electrodes consist of interconnected colloidal particles that enhance the internal surface area in comparison with conventional semiconductor electrodes. This has a significant impact on the TiO_2 electrochemical properties once reactions take place in the entire volume of the electrode. It is possible to adsorb a great amount of molecules on nanostructured TiO_2 surfaces, which is useful in electrochromic devices based on redox chromophores. The large specific surface area of nanostructured TiO_2 also allows a significant increase in the amount of absorbed dye-molecules, enhancing the efficiency of solar cells.[1] The small size of colloidal particles can lead to efficient charge separation upon illumination, which modifies the photoelectrocatalytic properties of TiO_2.[7] Nanostructured semiconductor characteristics can also increase the rate of diffusion of lithium ions within the material, which decrease in the response time of electrochemical windows not to mention that lithium batteries can supply high energy density on high current density.[4]

Although TiO_2 has eight polymorphs, the anatase phase has larger capacity to store lithium ions, together with a relatively high insertion/deinsertion rate.[4,8,9] The stability of electrolytic solutions in lithium-ion batteries is guaranteed with the presence of anatase TiO_2 at the negative electrode, which minimizes energy loss during the first cycles. Moreover, it is expected that the use of TiO_2 should decrease the risk of explosion in comparison with carbon and metallic lithium. Therefore, nanocrystalline TiO_2 (anatase) has suitable features that should allow its use in 2 V rocking-chair lithium battery, which seems to be more convenient than 4 V battery for application in microelectronic and consumer devices with photovoltaic recharging.[4]

The properties of anatase TiO_2 significantly depend on the details of its composition, preparation, and deposition methods, and several parameters still require optimization. There are numerous techniques for deposition of TiO_2 on glass,[10] such as the layer-by-layer (LbL) method. Several works have reported on the LbL films of TiO_2 nanoparticles, which have been used in electronic, electrochemical, and photocalytic systems.[11−16] Our interest lies in the production of LbL films of TiO_2 nanoparticles, in order to exploit desired electrochemical and electrochromogenic properties. Recent works have indicated that LbL films are promising for the production of electrochromic devices due to the film uniformity and to the possibility of controlling its thickness and nanoarchitecture.[17−23]

In this work, LbL films were prepared from TiO_2 nanoparticles and poly(vinyl sulfonic acid) (PVS). The choice of PVS was based on its stability in the commonly used potential range and on the fact that it is colorless due to the small amount of material that is deposited when using the LbL method. Thus,

[†] Ciências e Letras de Ribeirão Preto—Universidade de São Paulo.
[‡] Universidade Federal de São Carlos.
* E-mail: fritz@ffclrp.usp.br.

10.1021/jp064645i CCC: $33.50
Published on Web 11/14/2006

PVS serves as a good template material for the uniform growth of TiO_2 multilayers because of the electrostatic interactions between the sulfonic group and the positive charge on TiO_2 (at low pH values). Lithium insertion and deinsertion within the TiO_2/PVS LbL film are discussed on the basis of electrochemical and spectroelectrochemical results. The quadratic logistic equation (QLE) is used to describe the absorbance change (ΔA) as a function of the injected charge.[18,19,23] Finally, trapping and diffusion of charge carriers have been associated with the particle size, the amount of inserted lithium ion, and dissipation and feedback effects.

Experimental Section

The colloidal dispersion of anatase TiO_2 was prepared by hydrolysis of tetra-*n*-butyl titanate from Du-Pont (Tyzor). A mixture of 30 mL of the organic titanate and 30 mL of 2-propanol was slowly added (15 min) to 300 mL of deionized water under vigorous stirring. To this mixture was added 2 mL of a 70% nitric acid (under stirring). The resulting solution was stirred for 2 h at room temperature. The mixture was then heated to 80 °C under stirring for 4 h, giving rise to a stable and transparent (slightly cloudy) TiO_2 suspension (pH = 2). The effective diameter of the colloidal TiO_2 particles was 17.3 nm, as determined by dynamic light scattering (DLS) (Brookhaven Instruments Corp.). The dispersion was cooled, displayed no change in its transparency, and remained stable for at least 12 months. The anatase phase in the films prepared by this colloidal dispersion was detected by X-ray diffraction (XRD). The XRD of thin films, obtained after casting the TiO_2 dispersions onto the glass substrate, was recorded on a Siemens D5005 diffractometer using monochromatic Cu Kα radiation. The diffractogram displayed two diffraction peaks at 2θ values of 25° and 48°, which are characteristic of (101) and (200) of anatase TiO_2, respectively.[2] The commercial PVS was purchased from Aldrich.

LbL films were assembled onto a fluor-tin-oxide (FTO) coated glass purchased from Flexitec (Curitiba, Brazil), with sheet resistance of $\leq 20\ \Omega$. The layers were obtained via ionic attraction of oppositely charged materials, by alternated immersion of the FTO substrate into the TiO_2 and PVS (Aldrich) dispersions for 3 min. The concentration of PVS dispersion was 1.6 g L^{-1}, and pH = 2 was adjusted with HCl. After deposition of each layer, the substrates were rinsed in HCl solution for 30 s (pH = 2). The last layer of each LbL film was dried under a nitrogen flow. The colloidal TiO_2 dispersion employed herein and the method adopted for the growth of the self-assembled composites ensured formation of visually uniform films.

For the electrochemical and spectroelectrochemical experiments, the counter electrode was a platinum sheet with an area of 5 cm^2, and the quasi-reference electrode was saturated Ag/$AgNO_3$. An electrolytic solution of $LiClO_4$/propylene carbonate was used in all electrochemical experiments, which were carried out on an Autolab PGSTAT30 potentiostat/galvanostat. Chromogenic analysis was done simultaneously with the electrochemical experiments, by using a microprocessor-controlled solid-state light source (WPI, Inc.). Plastic fiber optic cables up to 1 mm in diameter were used to deliver red light (660 nm) from the instrument to a PDA1 photodiode amplifier (WPI, Inc.). The films were placed in a cell made of optical glass for the transmission experiments, where the light beams at fixed wavelengths were transmitted across the film during the cyclic voltammetry. Scanning electron microscopy (SEM) surface images were obtained on a digital Zeiss DSM 960 microscope. The thickness of the samples was measured with a Talystep profilometer.

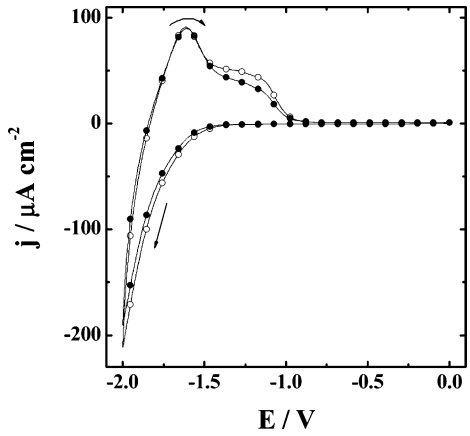

Figure 1. The 3rd (−○−) and 10th (−●−) cyclic voltammograms of 15-bilayer TiO_2/PVS LbL films. $\upsilon = 50$ mV s^{-1}.

Results and Discussion

Figure 1 displays the 3rd and 10th cyclic voltammograms for the 15-bilayer TiO_2/PVS LbL film obtained at a sweeping rate of 50 mV s^{-1}. Lithium insertion is depicted in the negative potential scan of these cyclic voltammograms, whereas the deinsertion process takes place during the positive potential scan. A voltammetric peak at ca. −1.6 V and a shoulder for potentials more positive than −1.5 V can be seen during the positive potential scan. The peak current corresponds to the oxidation of TiO_2 sites in the anatase phase, which reveals a quasireversible lithium deinsertion.[24] Meanwhile, the shoulders shown in the voltammograms must be associated with lithium deinsertion from another Li_xTiO_2 phase, which involves slow mobility of the charge carriers (lithium ions and/or electrons).

In Figure 1, it can also be observed that the voltammetric peak remains unchanged between the 3rd and 10th cyclic voltammograms. However, there is a decrease in the magnitude of the shoulder as a function of the number of voltammetric cycles, indicating trapping of charge carriers in the LbL film. The accumulation of Ti^{3+} and lithium ions is also responsible for the decrease in the cathodic current density as a function of the cycle number. It is noteworthy that the reduction in this current density is uniform for all the potential range where the electroreduction is observed ($E < -1.5$ V). This is different from what was observed for the electrooxidation process, where reduction of the current density occurred for a specific potential range ($-0.9\ \text{V} > E > -1.5$ V). This agrees with the decrease in the mobility of charge carriers after the first-order phase transition during the electroreduction process,[25−28] which hinders lithium deinsertion during the positive potential scan. Neutron diffraction data shown in the literature indicate that lithium insertion results in a phase transition from the tetragonal anatase (4-fold-coordination) structure toward the orthorhombic titanate (5-fold-coordination) phase to a stoichiometry of $Li_{0.5}TiO_2$.[26] Trapping of electrons at the surface is normally characterized by a small current peak or a small shoulder during the process of TiO_2 reduction,[29,30] which is not seen in the voltammograms of Figure 1. Thus, we believe that the self-assembled TiO_2 network consists of regions connected by energy barriers with different depths after the transition phase. So high-energy barriers require a longer time for electrons and/or lithium ions to overcome them.

Figure 2 displays cyclic voltammograms for 5-, 10-, 15-, and 20-bilayer TiO_2/PVS LbL films obtained at a sweeping rate of (a) 10 mV s^{-1}, (b) 50 mV s^{-1}, and (c) 200 mV s^{-1}. The shoulder width is enhanced in comparison with the peak width as the

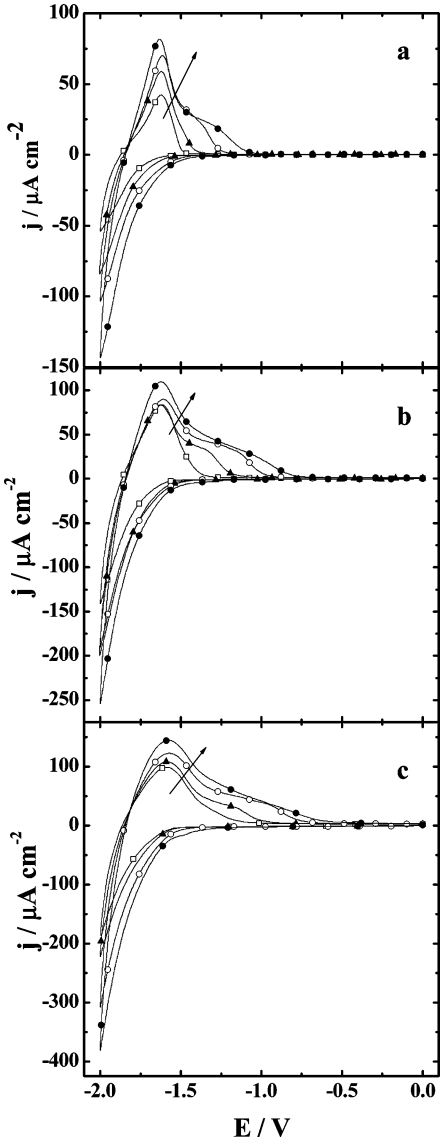

Figure 2. Cyclic voltammograms for (−□−) 5-, (−▲−) 10-, (−○−) 15-, and (−●−) 20-bilayer TiO_2/PVS LbL films, obtained at a sweeping rate of (a) 10 mV s^{-1}, (b) 50 mV s^{-1}, and (c) 200 mV s^{-1}. The arrow points to increasing number of bilayers, from 5 to 20.

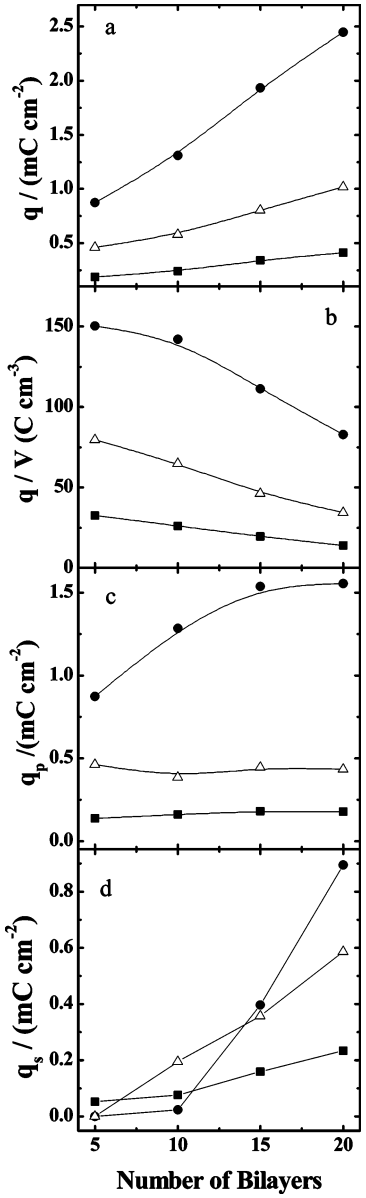

Figure 3. Values of (a) charge, (b) volumetric charge density, and (c) charge associated with the peaks and (d) with the shoulders in the voltammograms as a function of the number of bilayers, obtained at a sweeping rate of (●) 10 mV s^{-1}, (△) 50 mV s^{-1}, and (■) 200 mV s^{-1}.

number of bilayers increases from 5 to 20 and the sweeping rate changes from 10 mV s^{-1} to 200 mV s^{-1}. These results reveal the low mobility of charge carriers into the LbL film due to the trapping sites. It is also important to mention that the current density potentiodynamic profile for the TiO_2/PVS LbL films is similar to that of TiO_2 dipping films (not shown here), indicating that the presence of trapping sites are strictly associated with neither PVS nor the self-assembled method.

The charge for the lithium deinsertion process increases as the number of bilayers change from 5 to 20, indicating that the TiO_2/PVS LbL film grows up to 20 bilayers. The q values obtained at a sweeping rate of 10 mV s^{-1}, 50 mV s^{-1}, and 200 mV s^{-1} are shown in Figure 3a for 5, 10, 15, and 20 bilayers, respectively. Figure 3b shows the decrease in the volumetric charge density (charge per film volume) as a function of the number of bilayers, suggesting a low mobility of charge carriers into the TiO_2/PVS LbL film. The thickness measured for 5-, 10-, 15-, and 20-bilayer TiO_2/PVS LbL films was 58, 92, 174, and 296 nm, respectively. The geometrical area of all the LbL films was 1 cm^2.

Figures 3c−d display the charge associated with the voltammetric peak (q_p) and the shoulder (q_s) as a function of the number of bilayers at 10 mV s^{-1}, 50 mV s^{-1}, and 200 mV s^{-1}. The values of q_p and q_s were determined by the area of the Gaussian fitting of the voltammetric peaks and of the shoulders as a function of time, respectively. Note that the values of q_s increase in comparison with those of q_p as the number of bilayers changes from 5 to 20 bilayers. This means that the trapping effect increases with the number of bilayers.

Figure 4 shows the Nyquist diagrams for the 15-bilayers TiO_2/PVS LbL film subjected to several dc potentials with 5 mV of superimposed ac amplitude: (a) 0.0 V, −0.5 V, −1.0 V, and −1.25 V; (b) −1.5 V; (c) −1.7 V; (d) −1.9 V. Results in Figure 4a show semicircles associated with resistive and capacitive processes in parallel. These coupled processes are related to the interface, and they can be represented by the charge-transfer resistance (R_{ct}) and the double-layer capacitance (C_{dl}). R_{ct} values were determined by extrapolating the semicircle to the real axis, which decreased down to ca. 2.0 MΩ cm^2 as dc potentials

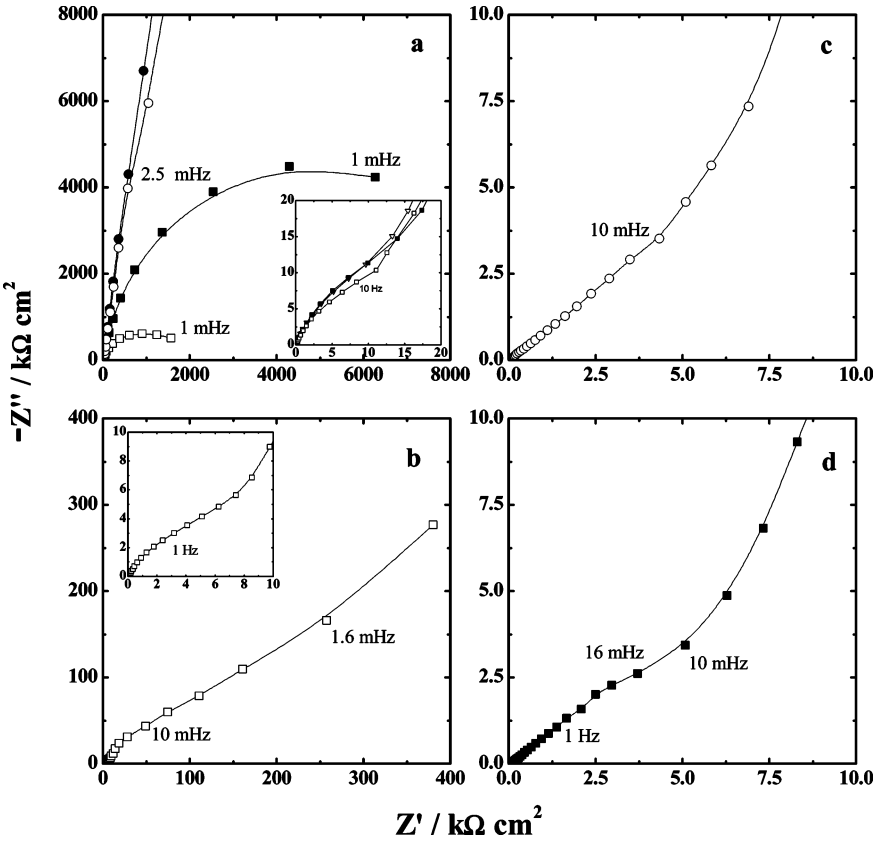

Figure 4. Nyquist diagrams for LbL film of 15 bilayers at (a) −0.5 V (−●−), −0.75 V (−○−), −1.0 V (−■−), and −1.25 V (−□−). In the inset: Nyquist diagrams for a range of high frequency at 0.0 V (−▽−), −1.0 V (−■−), and −1.25 V (−□−). (b) Nyquist diagrams at −1.5 V (−□−). In the inset: Nyquist diagrams for a range of high frequency at −1.5 V (−□−). Nyquist diagrams at (c) −1.7 V (−○−) and (d) −1.9 V (−■−).

changed from −1.0 V to −1.25 V. This means that the global reaction is controlled by activation in this potential range. The C_{dl} values for these potentials were ca. 10 μF cm^{-2}, which were determined by the complex plane of capacitance (not shown). In the inset, the plot shows the processes related to the bulk of the LbL film at 0.0 V, −1.0 V, and −1.25 V. Specifically, the beginning of the semicircle observed at frequencies higher than 10 Hz is associated with a couple between the bulk resistance (R_b) and the charge-space capacitance (C_{sc}). The R_b value was ca. 40 kΩ cm^2 at 0.5 V, which was determined by extrapolating the semicircle to low frequencies. There is a slight decrease in the R_b value between 0.0 V and −1.25 V. The values of charge-space capacitance changed slightly from 0.7 μF cm^{-2} to 0.8 μF cm^{-2} in this applied potential range.

Figure 4b shows a different profile of complex impedance in comparison with those plotted in Figure 4a. An overlap between the semicircles associated with interface process and lithium diffusion into the LbL film is observed, indicating that the global reaction rate at −1.5 V depends on these two processes. Note that the curve tends to capacitive behavior at low frequencies, indicating the finite diffusion process. The semicircle associated with R_b and C_{sc} at −1.5 V can still be seen in Figure 4b (inset). The bulk resistance is lower than those shown in Figure 4a (lower than 10 kΩ cm^2), and the charge-space capacitance is enhanced to ca. 6 μF cm^{-2}. These results are associated with the injection of electrons into the conduction band for $E_{dc} \leq -1.5$ V, as can be seen in the negative potential scan of the cyclic voltammograms shown in Figure 1.

For $E < -1.5$ V, the rate-limiting step is lithium diffusion ions into the LbL film, which is characterized by a straight line with a slope of ca. 45° with respect to the real axis. Figure 4c clearly shows this behavior for high frequencies. In Figure 4c, an increase in the phase angle can still be seen at low frequencies, which indicates there is a transition from the semi-infinite diffusion to finite diffusion. Note also that the bulk and charge-transfer resistances reached low values and cannot be observed at −1.6 V. In contrast, trapping of charge carriers into the network is observed in Figure 4d, which has already been discussed in the literature for intercalation electrodes.[31] A semi-infinite lithium diffusion can be noted for high frequencies as well as a time constant associated with the trapping process between 1 Hz and 1.6 mHz. The trapping effect is not observed in the cyclic voltammogram during the negative potential scan for the applied scan rates. The amount of electrons and lithium ions inserted into the LbL film in the steady-state at −1.9 V is sufficient to promote the first-order phase transition, and the formed phase adds an additional barrier to the charge transport activation energy.

On the basis of these electrochemical impedance spectroscopy data, we determined the diffusion coefficient of lithium ions (D) in according to the expression below, which is an alteration from that proposed by Ho et al.:[32]

$$|Z| = \left|\left(\frac{l}{\sqrt{2}D^{1/2}}\right)\left(\frac{dE}{dq}\right)\omega^{-1/2}\right| \quad (1)$$

where $|Z|$ is the impedance modulus, l is the thickness of the LbL film, ω is the angular frequency, and dE/dq is the potential slope as a function of the charge injected within the host matrix at the dc potential applied at 100 μV s^{-1}. The diffusion coefficient D changes from ca. 4.5 × 10^{-13} cm^2 s^{-1} to 3.0 × 10^{-14} cm^2 s^{-1} between −1.6 V and −2.0 V. Note that these D

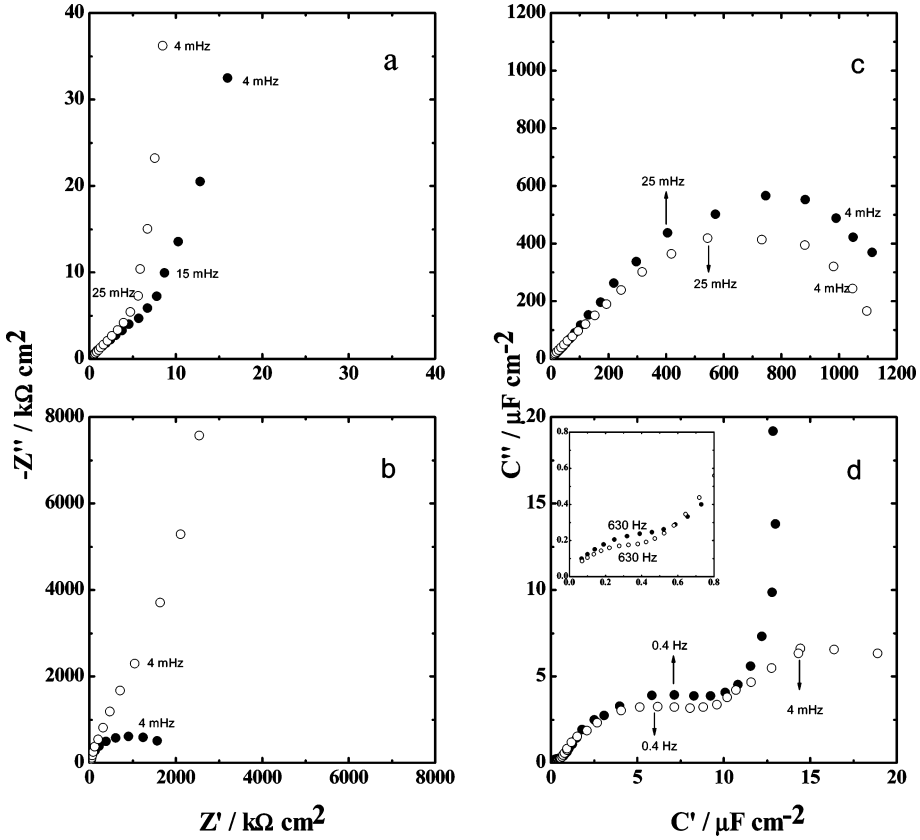

Figure 5. (a) Nyquist diagrams for LbL film of 15 bilayers for sequences (●) 1 and (○) 2 at (a) −1.6 V and (b) −1.25 V. Complex plane representation of the capacitance for sequences (●) 1 and (○) 2 at (c) −1.6 V and (d) −1.25 V.

values are similar to that observed in the literature for lithium insertion within the nanostructured TiO_2.[33] This means that PVS does not hinder the diffusion of lithium ions within the nanocomposite. Note also that the diffusion coefficient decreases with increasing injected charge. This fact is attributed to Li^+---Li^+ interactions, which also contribute to the decrease in ionic mobility into the film.[34]

Figure 5 shows the Nyquist diagram and the complex plane of capacitance at (a) −1.6 V and (b) −1.25 V for sequence 1 (from more positive to more negative dc potentials) and sequence 2 (from more negative to more positive *dc* potentials). The Nyquist diagrams obtained at −1.6 V for sequences 1 and 2 are similar. Semi-infinite and finite lithium diffusion processes into the LbL film are observed at high and low frequencies, respectively. However, the ionic mobility for sequence 2 is slightly higher than that for sequence 1. Observe that the finite diffusion for sequence 2 begins at a slightly higher frequency than that for sequence 1. The lithium diffusion coefficient at −1.6 V is 4.5×10^{-13} cm^2 s^{-1} and 1.7×10^{-13} cm^2 s^{-1} for sequences 1 and 2, respectively. This difference in *D* values is also seen in the literature,[32] and it is attributed to an additional activation for the insertion process due to lattice relaxation and/or removal of the solvation layer of the lithium ions to accommodate them into the host matrix. At −1.25 V, the Nyquist diagram for sequence 2 shows a significant difference in comparison with that of sequence 1. The profile of impedance data for sequence 2 is similar to that associated with the trapping of charge carriers into the network,[31] which has already been discussed above. This corroborates the results observed with the cyclic voltammograms.

Figure 5 shows the complex plane of capacitance at (c) −1.6 V and (d) −1.25 V for sequences 1 and 2. The capacitances associated with the diffusion process (C_o) are obtained by extrapolating the curves to the real axis for low frequencies. At −1.6 V, these values of C_o were ca. 1.15 mF cm^{-2} and 1.25 mF cm^{-2} for sequences 1 and 2, respectively. For the sequence 1 at −1.25 V, the complex plane of capacitance is associated with the double-layer capacitance and charge-space capacitance, which were obtained by extrapolating the semicircles to the real axis in Figure 5d and in the inset of Figure 5d, respectively. For sequence 2 at −1.25 V, Figure 5d shows the presence of an additional time constant in comparison with that for sequence 1. This semicircle observed for the low-frequency region is associated with the trapping of charge carriers, and its capacitance (C_t) is ca. 15 μF cm^{-2}. Comparing these results obtained under steady-state conditions with those from cyclic voltammetry, it is interesting to note that the trapping effect is still observed for potentials much less negative (at −1.25 V) than that for the ionic deinsertion from nontrapping sites (shown between ca. −1.9 V and −1.5 V in the voltammograms). This suggests that energy states must be formed because of a strong structural perturbation into the TiO_2 host promoted by the electroinsertion of lithium ions, as will be seen below.

Figure 6a shows the potentiodynamic profile for the absorbance change (ΔA) at different wavelengths: 525, 590, 623, and 660 nm. These spectroelectrochemical data were obtained in situ with the cyclic voltammogram at 50 mV s^{-1} for 15-bilayer TiO_2/PVS LBL films. The largest absorbance change and the greatest electrochromic efficiency ($\eta = \Delta A/q$) are observed at 660 nm. The η values for the applied potential range is 3.4, 4.8, 7.3, and 8.9 cm^2 C^{-1} at the wavelengths 525, 590, 623, and 660 nm, respectively. However, the electrochromic efficiency is not constant for all applied potential range. For instance, the electrochromic efficiency for the potential range associated with the voltammetric peak is greater (13.1 cm^2 C^{-1})

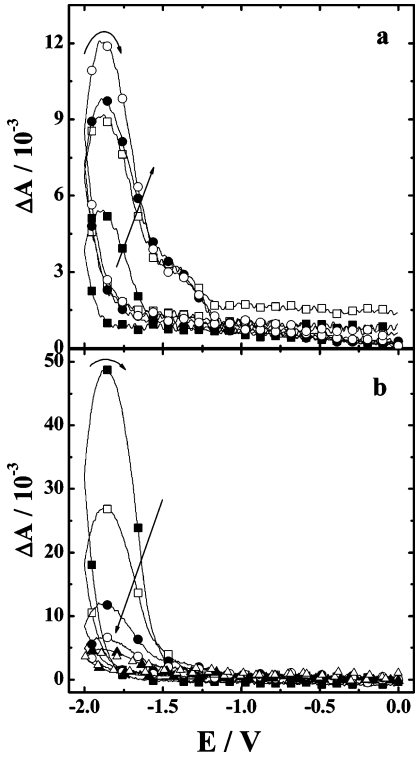

Figure 6. (a) Absorbance changes, ΔA, at (−■−) 525 nm, (−□−) 590 nm, (−●−) 623 nm, and (−○−) 660 nm for 15-bilayer LBL films. The arrow points to increasing wavelength, from 525 to 660 nm. (b) Absorbance changes at 660 nm for various scan rates: $v = 10$ mV s^{-1} (−■−), 20 mV s^{-1} (−□−), 50 mV s^{-1} (−●−), 100 mV s^{-1} (−○−), 150 mV s^{-1} (−▲−), and 200 mV s^{-1} (−△−). The arrow points to increasing scan rate, from 10 to 200 mV s^{-1}.

than that observed for the potential range related to the shoulder (4.4 cm^2 C^{-1}) at 660 nm during the positive potential scan.

Figure 6b shows the potentiodynamic profile of the absorbance change at 660 nm for the 15-bilayer TiO_2/PVS LbL film at several scan rates. As expected, there is a decrease in the absorbance change as a function of the scan rate due to the slow diffusion of lithium ions during the insertion process. On the basis of these spectroelectrochemical data, we plotted the absorbance change as a function of the charge associated with ionic deinsertion (Figure 7) at (a) 20, (b) 50, and (c) 200 mV.s^{-1}. It can be clearly seen that the curve slope is changed during the deinsertion process. This difference in the electrochromic efficiency is associated with the different electronic transitions between the energy bands of TiO_2. In Figure 7a, it can be observed that the curve slope is increased for a charge more positive than 0.8 mC cm^2. The absorbance change for $q > 0.8$ mC cm^{-2} is assigned to intra- and interband transitions related to the electron density in the conduction band.[29,35] The η values associated with these delocalized charge carriers are close to those reported in the literature.[30] Meanwhile, the absorbance change associated with the oxidation process involving trapping of the TiO_2 sites ($q < 0.8$ mC cm^{-2}) is attributed to electronic transitions involving energy states in the gap band, which are formed due to strong perturbation in the anatase structure during the insertion of lithium ions. Note that the profile of ΔA vs q is a typical intervalence charge transfer, which can be seen clearly at high scan rates (Figure 4b,c). Thus, there is an electron transfer from the energy levels in the gap band to the neighboring Ti^{4+} sites.

The absorbance change follows the Lambert−Beer law during the lithium deinsertion process for high q values:

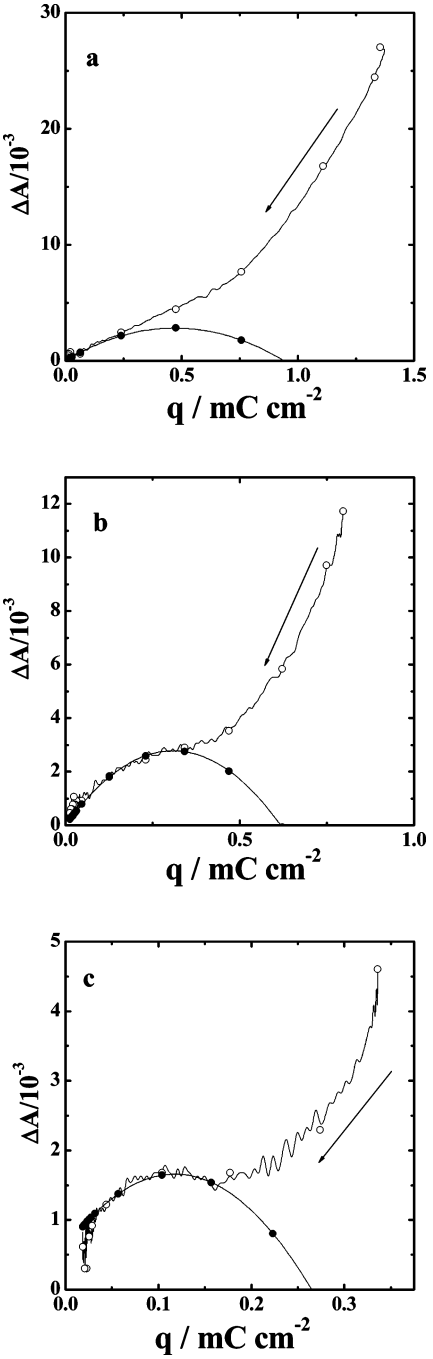

Figure 7. Plot of the theoretical (−●−) and experimental (−○−) ΔA data at 660 nm as a function of the charge for the 15-bilayer TiO_2/PVS LbL films at (a) 20 mV s^{-1}, (b) 50 mV s^{-1}, and (c) 200 mV s^{-1}.

$$\Delta A = \epsilon l \Delta C \tag{2}$$

where ϵ is the molar absorption coefficient, l is the thickness of the film, and C is the concentration of the absorbent species in mol cm^{-3}, which can be associated with the charge injected:

$$q = znF \tag{3}$$

where n is the number of moles of redox species per unit area, z is the charge of this species, and F is the Faraday's constant. So q/zF is equivalent to $l\Delta C$, and ϵ can be related by:

$$\Delta A = q\frac{\epsilon}{zF} \tag{4}$$

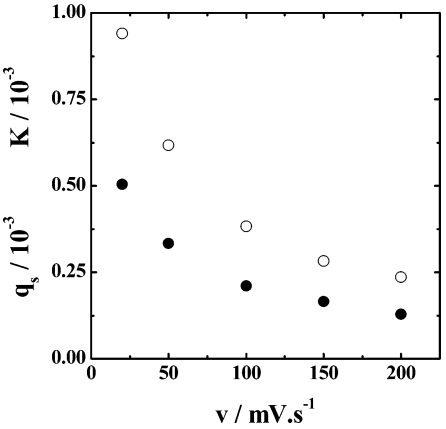

Figure 8. Plot of the values of (●) q_s and (○) K as a function of the scan rate.

However, a term due to the negative feedback effect for absorbance change as a function of the charge must be included in eq 4, as observed in Figure 7 for low q values. In this context, QLE is used to describe the temporal evolution of the electron number ($N_{Ti(III)\rightarrow Ti(IV)}$) participating in the intervalence transfer from Ti^{3+} to Ti^{4+} in the LbL films. QLE is expressed as

$$\frac{dq}{dt} = sq\left(1 - \frac{q}{K}\right) \tag{5}$$

where s is a positive constant and K is associated with the ability of the system to sustain the growth of $N_{Ti(III)\rightarrow Ti(IV)}$. The term $(1 - q/K)$ represents the effects from dissipation and feedback, which increase with q. Equation 5 can still be substituted by eq 6:

$$\Delta A = rq\left(1 - \frac{q}{K}\right) \tag{6}$$

In this case, it is implied that r is associated with the molar absorption coefficient ($= \epsilon/zF$) and ΔA is related to dq/dt. The magnitude of the absorbance depends on the frequency of the charge (electron) transfer between the Ti^{3+} and Ti^{4+} sites, in addition to the dependence on the amount of injected charge. The electrons that participate in this charge-transfer process are those injected electrochemically. As the charge injected increases, so does the number of transferred electrons from Ti^{3+} to Ti^{4+} sites and the number of intercalated ions, which are transported simultaneously to maintain the electroneutrality. This increase leads to interactions between the charge carriers themselves, and to interactions between the charge carriers and the network (trapping sites), with the appearance of dissipative forces. At the same time, the dissipation effect increases with the increasing number of charge carriers, contributing to the feedback effect. In other words, the dissipative forces opposing the electron transfer increase with the amount of charge carriers, thus decreasing the electrochromic efficiency.[18,19, 23]

The total number of trapping TiO_2 sites can be probed by monitoring the light absorption associated with the intervalence transfer from Ti^{3+} to Ti^{4+} sites. The absorbance change associated with the intervalence transfer is null as the charge inserted reduces all the Ti^{4+} sites to trapping Ti^{3+} sites (or as the deinserted charge oxidizes all the trapping Ti^{3+} sites to Ti^{4+} sites). The value of this charge is equal to K, whose value was obtained by fitting Figure 7 with eq 6. Figure 8 shows K and q_s values of as a function of the scan rate. Note that K decreases as the scan rate changes from 20 to 200 mV s^{-1}. This is associated with slow diffusion of the lithium ions during the insertion process, thus limiting the access of lithium ions to the sites at the film/electrolytic solution interface, at high scan rates. It is also noted that the ratio between q_s and K is about 0.55, which corresponds to a stoichiometry of $Li_{0.55}TiO_2$ for the trapping sites. This maximum ambient-temperature lithium insertion is about similar to that observed in the literature for crystal anatase TiO_2.[33] So, we believe that trapping sites are formed after phase transition because the stoichiometry is about $Li_{0.55}TiO_2$. This gives rise to energy levels in the gap band that are responsible for the intervalence transfer absorbance.

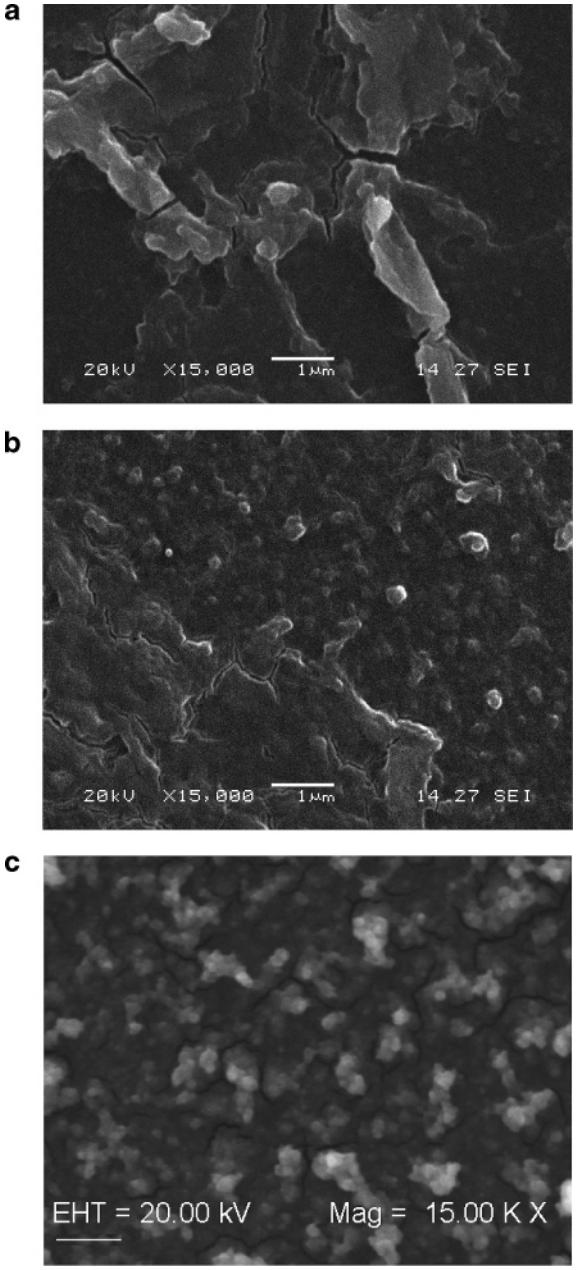

Figure 9. Scanning electron micrographs for (a) 5-, (b) 15-, and (c) 20-bilayer TiO_2/PVS LbL films. Scale bar = 1 μm.

Figure 9 shows scanning electron micrographs (at 15 000×) of the TiO_2/PVS LbL film with (a) 5, (b) 15, and (c) 20 bilayers. It can immediately be seen that both LbLs are cracked and have a large amount of roughly spherical colloidal particles with mean diameters close to 160 nm. This increase in the mean diameter of the particles in the LbL film, in comparison with that in colloidal dispersion, is probably associated with a change in the surface charge of the particles during the self-assembly

process, leading to their agglomeration. It can also be noted in Figure 9 that the amount of colloidal particles increases as a function of the number of bilayers. This fact can be related with the enhancement in the ratio between the charge associated with trapping sites (q_s) and that associated with nontrapping sites (q_p) as the number of bilayers increase from 5 to 20 bilayers (Figure 3).

The mean time for the diffusion of lithium ions within colloidal particles ($\langle t \rangle_c$) and within compact layers ($\langle t \rangle_l$) are given respectively by[4]

$$\langle t \rangle_c = \frac{d^2}{4\pi D} \tag{7}$$

$$\langle t \rangle_l = \frac{l^2}{2D} \tag{8}$$

Based on eqs 7 and 8, $\langle t \rangle_c$ will be equal to $\langle t \rangle_l$ as

$$d = \sqrt{2\pi} l \tag{9}$$

where d is the diameter of the colloidal particles. Considering a thickness of 58 nm for the 5-bilayer LbL film, the diameter of the colloidal particles in these LbL films should be equal to 145 nm, since the molar ratio of lithium-to-titanium ions is similar for the colloidal particles and the compact layer. As the mean diameter value (ca. 160 nm) is close to 145 nm, the $Li_{0.55}TiO_2$ composition must be reached almost simultaneously in the colloidal particles and in compact layers of the 5-bilayer LbL film. As the trapping effect occurs for the $Li_{0.55}TiO_2$ composition and this effect is not observed in the voltammograms of the 5-bilayer LbL film, we believe that the colloidal particles may be responsible for the trapping of charge carriers and that the amount of colloidal particles is minimum for the 5-bilayer LbL film and increases toward the 20-bilayer LbL film. This reasoning is reinforced by the results obtained for the 20-bilayer LbL film, which has the largest trapping effects among the LbL films studied here. The $Li_{0.55}TiO_2$ composition is probably reached faster in the colloidal particles than in the compact layers for the 20-bilayer LbL film ($l = 296$ nm), and the scanning electron micrographs give evidence of a larger amount of colloidal particles for the LbL film with this number of bilayers.

A first-order phase transition from the tetragonal anatase structure toward the orthorhombic titanate phase to a stoichiometry of $Li_{0.5}TiO_2$ is well documented in the literature.[26] However, this phase transition cannot be responsible for the trapping effects in compact layers. On the basis of the results shown in this paper, there is good evidence that the trapping of charge carriers occurs in colloidal particles only, after a first-order phase transition.

Conclusions

The electrostatic interactions between the colloidal particles of TiO_2 and PVS allow the growth of visually uniform LbL films. The presence of PVS does not hinder the lithium diffusion within the LbL film, serving only for the construction of self-assembled matrixes. The high control of the nanoarchitecture in these LbL films allows a better understanding of the electrochemical and spectroelectrochemical properties. Scanning electron micrographs have shown that the film consists of cracked regions and colloidal particles with a mean diameter close to 160 nm. Moreover, on the basis of the thickness of the film and the charge (q) as a function of the number of bilayers, the trapping of charge carriers observed during the cyclic voltammetry was attributed to the colloidal particles. Absorbance change associated with the trapping sites involves intervalence transfer from Ti^{3+} to Ti^{4+} and energy levels into the gap band due to a strong structural perturbation. The interactions between the charge carriers and between the charge carriers and the TiO_2 nanoparticles are responsible for dissipation and feedback effects, as predicted by the QLE. The use of this equation gives an estimate of the amount and composition of trapping sites, which must be formed after a first-order phase transition, as the molar ratio of lithium-to-titanium ions in the colloidal particles is close to 0.55.

Acknowledgment. N.A.G. thanks FAPESP for the scholarship (no. 2005/01877-7). We are grateful to FAPESP (Proc. no. 05/00106-7) and CNPq (Proc. no. 55.0581/2005-7) for the financial support. We are also grateful to Professor Ernesto R. Gonzalez (IQSC/USP) and Dr. Herenilton Oliveira (FFCLRP/USP) for spectroelectrochemical experiments.

References and Notes

(1) O'Regan, B.; Grätzel, M. *Nature* **1991**, *353*, 737.
(2) Ghicov, A.; Tsuchiya, H.; Hahn, R.; Macak, J. M.; Munõz, A. G.; Schmuki, P. *Electrochem. Commun.* **2006**, *8*, 528.
(3) Georg, A.; Georg, A.; Krašovec, U. O. *Thin Solid Films* **2006**, *502*, 246.
(4) Exnar, E.; Kavan, L.; Huang, S. Y.; Grätzel, M. *J. Power Sources* **1997**, *68*, 720.
(5) Kiyonaga, T.; Mitsui, T.; Torikoshi, M.; Takekawa, M.; Soejima, T.; Tada, H. *J. Phys. Chem. B* **2006**, *110*, 10771.
(6) O'Regan, B. C.; Durrant, J. R. *J. Phys. Chem. B* **2006**, *110*, 8544.
(7) Hoffmann, M. R.; Martin, S. T.; Choi, W.; Bahnemann, D. W. *Chem. Rev.* **1995**, *95*, 69.
(8) Wilhelm, O.; Pratsinis, S. E.; de Chambrier, E.; Crouzet, M.; Exnar, I. *J. Power Sources* **2004**, *134*, 197.
(9) Lindström, H.; Södergren, S.; Solbrand, A.; Rensmo, H.; Hjelm, J.; Hagfeldt, A.; Lindquist, S.-E. *J. Phys. Chem. B* **1997**, *101*, 7710.
(10) Sankapal, B. R.; Lux-Steiner, M. Ch.; Ennaoui, A. *Appl. Surf. Sci.* **2005**, *239*, 165.
(11) Kovtyukhova, N.; Ollivier, P. J.; Chizhik, S.; Dubravin, A.; Buzaneva, E.; Gorchinskiy, A.; Marchenko, A.; Smirnova, N. *Thin Solid Films* **1999**, *337*, 166.
(12) Cassagneau, T.; Fendler, J. H.; Mallouk, T. E. *Langmuir* **2000**, *16*, 241.
(13) Kim, T.-H.; Sohn, B.-H. *Appl. Surf. Sci.* **2002**, *201*, 109.
(14) Kim, J. H.; Kim, S. H.; Shiratori, S. *Sens. Actuators B* **2004**, *102*, 241.
(15) He, J.-A.; Mosurkal, R.; Samuelson, L. A.; Li, L.; Kumar, J. *Langmuir* **2003**, *19*, 2169.
(16) Paddon, C. A.; Marken, F. *Electrochem. Commun.* **2004**, *6*, 1249.
(17) DeLongchamp, D. M.; Hammond, P. T. *Chem. Mater.* **2004**, *16*, 4799.
(18) Huguenin, F.; Gonzalez, E. R.; Oliveira, O. N., Jr. *J. Phys. Chem. B* **2005**, *109*, 12837.
(19) Huguenin. F.; Zucolotto, V.; Carvalho, A. J. F.; Gonzalez, E. R.; Oliveira, O. N., Jr. *Chem. Mater.* **2005**, *17*, 6739.
(20) Huguenin, F.; Ferreira, M.; Zucolotto, V.; Nart, F. C.; Torresi, R. M.; Oliveira, O. N., Jr. *Chem. Mater.* **2004**, *16*, 2293.
(21) Ferreira, M.; Huguenin, F.; Zucolotto, V.; da Silva, J. E. P.; de Torresi, S. I. C.; Temperini, M. L. A.; Torresi, R. M.; Oliveira, O. N., Jr. *J. Phys. Chem. B* **2003**, *107*, 8351.
(22) Huguenin, F.; dos Santos, D. S.; Bassi, A.; Nart, F. C.; Oliveira, O. N., Jr. *Adv. Funct. Mater.* **2004**, *14*, 985.
(23) Huguenin, F.; Nart, F. C.; Gonzalez, E. R.; Oliveira, O. N., Jr. *J. Phys. Chem. B* **2004**, *108*, 18919.
(24) Kavan, L.; Fattakhova, D.; Krtil, P. *J. Electrochem. Soc.* **1999**, *146*, 1375.
(25) Kavan, L.; Kratochvilovfi, K.; Grätzel, M. *J. Electroanal. Chem.* **1995**, *394*, 93.
(26) Cava, R. J.; Murphy, D. W.; Zahurak, S.; Santoro, S.; Roth, R. S. *J. Solid State Chem.* **1984**, *53*, 64.
(27) Dinh, N. N.; Oanh, N. Th. T.; Long, P. D.; Bernard, M. C.; Goff, A. H.-L. *Thin Solid Films* **2003**, *423*, 70.
(28) van de Krol, R.; Goossens, A.; Meulenkamp, E. A. *J. Appl. Phys.* **2001**, *90*, 2235
(29) Boschloo, G.; Fitzmaurice, D. *J. Phys. Chem. B* **1999**, *103*, 7860.
(30) Boschloo, G.; Fitzmaurice, D. *J. Phys. Chem. B* **1999**, *103*, 2228.
(31) Bisquert, J.; Vikhrenko, V. S. *Electrochim. Acta* **2002**, *47*, 3977.

(32) Ho, C.; Raistrick, I. D.; Huggins, R. A. *J. Electrochem. Soc*. **1980**, *127*, 345.
(33) Kavan, L.; Grätzel, M.; Gilbert, S. E.; Klemenz, C.; Scheel, H. J. *J. Am. Chem. Soc.* **1996**, *118*, 6716.
(34) Baddour, R.; Pereira-Ramos, J. P.; Messina, R.; Perichon, J. *J. Electroanal. Chem.* **1991**, *314*, 81.
(35) Rothenberger, G.; Fitzmaurice, D.; Grätzel, M. *J. Phys. Chem.* **1992**, *96*, 5983.